Preparation of tunable-sized iron nanoparticles based on magnetic manipulation in inert gas condensation (IGC)

Xing, Lijuan; ten Brink, Gert H.; Kooi, Bart J.; Palasantzas, George

Published in:
Journal of Applied Physics

DOI:
10.1063/1.4974052

Preparation of tunable-sized iron nanoparticles based on magnetic manipulation in inert gas condensation (IGC)

Lijuan Xing, Gert H. ten Brink, Bart J. Kooi, and George Palasantzas

Citation: Journal of Applied Physics **121**, 024305 (2017); doi: 10.1063/1.4974052
View online: http://dx.doi.org/10.1063/1.4974052
View Table of Contents: http://aip.scitation.org/toc/jap/121/2
Published by the American Institute of Physics

Preparation of tunable-sized iron nanoparticles based on magnetic manipulation in inert gas condensation (IGC)

Lijuan Xing,[a] Gert H. ten Brink, Bart J. Kooi, and George Palasantzas
Zernike Institute for Advanced Materials, University of Groningen, Nijenborgh 4, 9747 AG Groningen, The Netherlands

(Received 24 October 2016; accepted 3 January 2017; published online 13 January 2017)

Iron nanoparticles (NPs) prepared by inert gas condensation were studied using high resolution transmission electron microscopy and Wulff construction shape analysis. The NP size and shape show strong dependence on the magnetic field above the target surface. The effect of the magnetic field could be tuned by adjusting the thickness of the protective backing plate positioned in-between the target and the magnetron head. With increasing backing plate thickness, the particle size decreases and the NP morphologies evolve from faceted to close-to-spherical polyhedral shapes. Moreover, with changes in size and shape, the particle structure also varies so that the NPs exhibit: (i) a core-shell structure for the faceted NPs with size ∼15–24 nm; (ii) a core-shell structure for the close-to-spherical NPs with size ∼8–15 nm; and (iii) a fully oxidized uniform structure for NPs with sizes less than ∼8 nm having a void in the center due to the Kirkendall effect. The decrease of NP size with the increasing backing plate thickness can be attributed to a reduced magnetic field strength above the iron target surface combined with a reduced magnetic field confinement. These results pave the way to drastically control the NP size and shape in a simple manner without any other adjustment of the aggregation volume within the deposition system. *Published by AIP Publishing*. [http://dx.doi.org/10.1063/1.4974052]

I. INTRODUCTION

Fe and Fe oxide nanoparticles (NPs) are considered promising nanomaterials for applications in a variety of key fields from data storage,[1] catalysis,[2,3] and ground water remediation[4] to drug delivery,[5,6] magnetic resonance imaging (MRI) contrast enhancement, and hyperthermia.[7–9] NPs, as is well known, exhibit properties that can be tremendously distinct from their macroscopic counterparts,[10] and the properties as well as surface chemistry then show strong sensitivity to particle size and shape.[11,12] The size-dependent properties can originate from the high surface-to-volume ratio, and influences by particle shapes can be attributed to the distinct crystallographic surfaces that enclose the NP.[13] Therefore, in order to optimize the performance for a specific application, it is of crucial importance to control precisely the particle size, structure, and morphology.

So far, a wide range of techniques have been applied to produce NPs, including thermal decomposition,[14–16] chemical vapor condensation,[17] gas evaporation method,[18] and inert gas condensation.[19,20] The vacuum techniques are now extensively used in the preparation of NPs as they provide a convenient method to produce solvent-free NPs. The inert gas condensation system used in our work is a combination of magnetron sputtering and inert gas condensation. The design concept of the system originates from the study of Haberland[21] who first applied the plasma sputtering technique in a cluster source instead of previously used thermal evaporation. Besides high purity, NPs prepared by inert gas condensation also possess a higher diversity of crystal motifs in comparison to chemical techniques as is shown in a recent report,[22] where we described size dependent core-shell structured Fe NPs. In any case, the formation of NPs starts with sputtering, which is the ejection of surface and near-surface atoms from target materials caused by the bombardment of energetic particles.[23] In the case of inert gas condensation, sputtering commences when positive ions of the working gas (Ar), which are formed by collisions with electrons, are accelerated towards and impact the target surface due to the potential difference between the cathode (material target) and anode (magnetron cover).

Nevertheless what remains a problem for the preparation of magnetic NPs, e.g., Fe NPs in our work, are a weakened sputtering (due to the strong magnetic field of the target) and the under-utilization of the magnetic target. To remedy these issues, we introduced a copper (Cu) backing plate in between the target and the magnetron to virtually shift the magnetic field distribution above the target surface. The aim is to further decrease the minimum NP size that can be obtained by this technique based on the fact that the magnetic field configuration influences the cluster formation process enormously.[24–26] Compared with the originally strong magnetic field, in the absence of a backing plate, the target will feel a lower magnetic field resulting in a weakened plasma confinement and a broader target erosion zone. Furthermore, it should be noted that the total thickness (of the Fe target and the backing plate) should be limited to a level that still enables a sufficient magnetic field (typically ∼200–250 G) to be projected over the sputter target surface to ensure magnetron sputtering.[27] We will show in the present work that the use of backing plates affords a feasible method to decrease the NP size in inert gas condensation besides the widely used

[a]Author to whom correspondence should be addressed. Electronic mail: l.xing@rug.nl

control through regulating the aggregation length,[25] gas flow[28] as well as the discharge current,[29] and the target utilization under the weakened magnetic field can be further improved. The modified magnetic field configuration not only broadens the attainable range of particle sizes for a selected target material but also promotes the particle shape and structure to experience great changes with varied size associated by the use of different backing plates.

II. EXPERIMENTAL METHODS

Fe NPs were deposited directly onto holy carbon-coated transmission electron microscopy (TEM) grids with a home modified high pressure magnetron sputtering source (see supplementary material for the NP deposition system in Fig. S1). A Cu backing plate (diameter 50.8 mm, thickness varying between 0.5 and 2 mm) was installed between the Fe target (diameter 50.8 mm, thickness 0.5 mm, purity 99.9%) and the magnetron. The sample chamber was evacuated to a base pressure of $\sim 10^{-8}$ mbar (aggregation chamber: $\sim 10^{-6}$ mbar). The applied sputtering current was 0.2 A, and the aggregation length was adjusted between 5 and 8 cm (magnetron head-exit aperture distance) by using a linear motion drive. Supersaturated Fe vapor was produced by magnetron sputtering of the Fe target in an inert gas atmosphere of Ar and minute amounts of CH_4. The latter was used to achieve system pressures $\sim 10^{-5}$ mbar, yielding a reducing gas environment,[22] prior to inert gas insertion and subsequent magnetron sputtering. The supersaturated Fe vapor is then mainly cooled by collision with Ar ions forming NP nuclei, and subsequently the desired size NPs. The formed NPs in the aggregation chamber were then carried by Ar (sputtering gas) to the sample chamber leading to soft landing (without NP deformation) onto various substrates. Fe nanoparticles exposed to ambient conditions (e.g., during transfer to TEM) forming a thin oxide layer surrounding the Fe core or a fully oxidized structure for small particles.[21]

III. RESULTS AND DISCUSSION

Figure 1 shows an overview of TEM images for Fe NPs (left column) prepared with Cu backing plate thicknesses varying from 2.0 mm to 0.5 mm, which reveals an obvious size and morphology evolution with the increasing thickness of the backing plate. The corresponding size distributions are also shown in the right column with the mean size, standard deviation, and typical morphologies observed included as well. In any case, Figure 1 demonstrates that with increasing backing plate thickness, the particle size shows a clear decrease, and the morphology experiences an evolution from faceted to close-to-spherical polyhedral shapes. On the other hand, the particle structure varies with the change of size and shape: NPs exhibit a core-shell structure for faceted NPs as well as close-to-spherical particles larger than ~8 nm; however, a fully oxidized uniform structure is formed with a void in the center due to the Kirkendall effect[30,31] for near-spherical particles smaller than ~8 nm.

The core-shell structured NP is constituted by an iron core and an oxide shell with a thickness of ~2–3 nm, which has been concluded from high resolution transmission electron

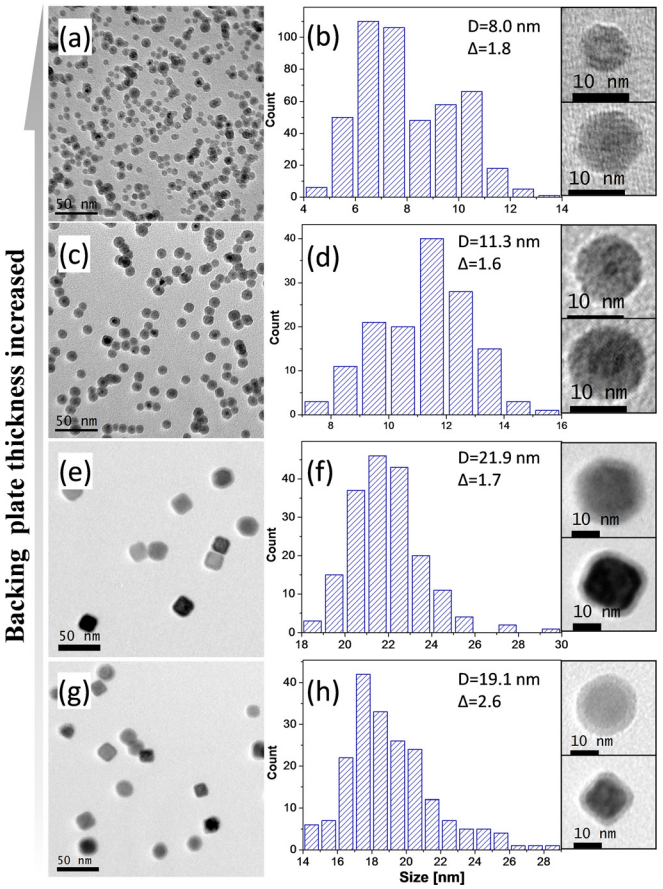

FIG. 1. Overview TEM images (left column) and the corresponding size distribution (middle column) and typical particle morphologies (right column, based on statistics of numerous areas) of Fe NPs deposited on holey carbon grids prepared with different backing plate thicknesses: (a) and (b) 2.0 mm, (c) and (d) 1.5 mm, (e) and (f) 1.0 mm, (g) and (h) 0.5 mm, respectively. NPs with different sizes adopt different structures and morphologies: (i) Particles smaller than 8 nm are fully oxidized forming a spherical structure with a hole in the center (upper shape in (b)); (ii) medium sized particles (~8–15 nm) show a close-to-spherical shape with a pure Fe core (lower shape in (b) and both shapes in (d)); (iii) particles with a size larger than 15 nm possess faceted shapes with an Fe core, i.e., rhombic dodecahedra (upper shapes in (f) and (h)) and truncated cubes (lower shapes in (f) and (h)).

microscopy (HRTEM) analysis in the previous report,[22] revealing no systematic dependence on the particle size.[32,33] The oxide layer consists of Fe_3O_4 (magnetite) or γ-Fe_2O_3 (maghemite) or a combination of both. For body centered cubic (bcc) structured Fe, particles tend to adopt a faceted shape (as it is shown in Figures 1(f) and 1(h) for particles larger than ~15 nm). Based on the Cabrera-Mott theory, once an oxide layer initially formed surrounding the NP, transport of electrons from the iron core to the adsorbed oxygen through the oxide layer allows the oxidation to continue.[31] This establishes a strong electric field within the NP that is able to drive the ion diffusion. With the influence of the electric field, Fe cations move towards the particle surface and O anions move towards the core. As the oxidation proceeds, the particle shape gradually approaches a close-to-spherical morphology. This is depicted by the smaller particles with sizes ~8–15 nm in Figure 1(c) that show a near-spherical polyhedral shape with a core-shell structure. When the oxidation proceeds further, the influence from the imbalance in the relative rates for the outward diffusion of Fe and the inward diffusion of O[29,34]

dramatically emerges, leading to a reduced intensity region in the center for fully oxidized NPs. This is observed in Figures 1(a) and 1(b), indicating the presence of a void resulting from the Kirkendall effect.[30,31]

Figure 2 shows clearly the size evolution with the thickness of the backing plate introduced in the magnetron head. The faceted morphologies observed for particles larger than ~15 nm, i.e., truncated cube (TC) and truncated rhombic dodecahedron (TRD), are presented as insets. The truncated cubic NPs are enclosed by 6 {100} planes and truncated by 12 {110} planes; the truncated rhombic dodecahedra are confined by 12 {110} planes and truncated by 6 {100} planes. For Fe with a bcc structure, these distinct crystal morphologies are formed owing to different values of the ratio R of the growth speed along the ⟨100⟩ and ⟨110⟩ directions.[22]

The "*easy-to-sputter*" trend of NPs and the smaller NPs observed with the backing plate in between the target and the magnetron can be attributed to a weakened magnetic field above the target surface combined with a reduced magnetic field confinement. Indeed, Figure 3(a) demonstrates the basic magnetron design used in the plasma sputtering system in section. The magnetic field configuration is illustrated in Figure 3(b) and target arrangements without (left) and with (right) backing plates are depicted, respectively. The corresponding race-tracks observed on the sputtered Fe target are shown in Figure 3(c). The magnetron is principally composed of a cylindrical magnet in the center surrounded by an annular magnet. To move the target further away from the magnetron (by adjusting the thickness of the backing plate) will definitely result in a weaker magnetic effect from the magnetron and a lower interference from the magnetic Fe target as well. Overall, a decreased magnetic field projection upon the Fe target is obtained by using the backing plates, which is confirmed by the wider race-track that is observed on the target after the deposition, as it is shown in Figure 3(c).

During the process of plasma sputtering, a fraction of the free metal atoms are ionized, and a stronger magnetic field results in a higher fraction of ionized atoms, which can

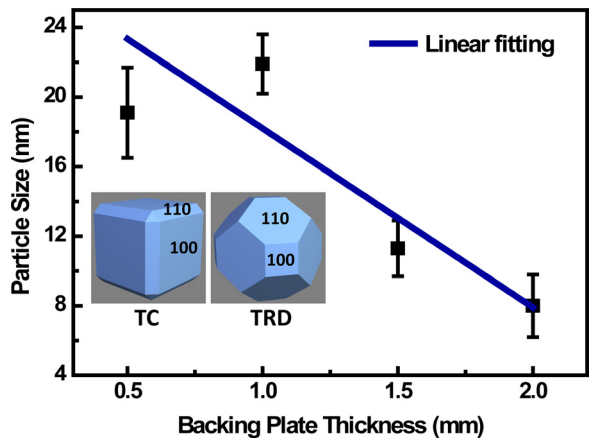

FIG. 2. Evolution of the average NP size with varied backing plate thickness. The observed faceted morphologies of truncated cube (TC) and truncated rhombic dodecahedron (TRD) for particles larger than ~15 nm are reconstructed using the Wulff construction. A linear fitting of the form $D = p + qt$ (with fitting parameters $p = 28 \pm 5.6$, $q = -10 \pm 3.9$, $R^2 = 0.67$) is shown to indicate qualitatively the variation tendency of the particle size.

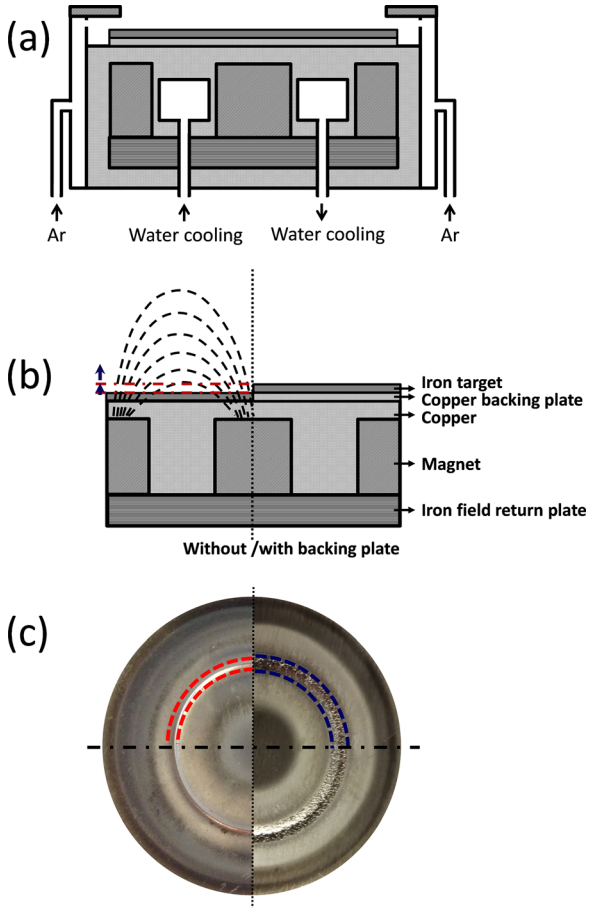

FIG. 3. The basic magnetron design that is used in the NP deposition system is shown in cross-section in (a). The magnetic field configuration is described in (b), and different target arrangements are depicted in the left without backing plate, and in the right with backing plate. The red dashed dotted lines indicate the surface position of the sputter Fe target, which shows a shift to a weaker magnetic field location when the target moves away from the magnetron owing to the installation of the backing plate (see the lower arrow). By changing the thickness of the backing plate, the target surface can move further following the upper arrow direction so that the projected magnetic field strength can be further reduced. Fe targets after sputtering without (left) and with (right) a backing plate are shown in (c), the race-tracks of which are marked with red and blue dashed lines, respectively. A wider race-track (marked with the blue dashed lines), which is resulted from the weakened magnetic field strength, can be observed with the baking plate present in between the Fe target and the magnetron head.

electrically influence the cluster nucleation and the subsequent growth dynamics. In the initial stage of NP formation, a three-body collision ($2Fe + Ar \rightarrow Fe_2 + Ar$) is necessary in the inert gas atmosphere to form the nucleus, releasing the latent heat of condensation simultaneously to conserve the energy and momentum of the entire system.[29,35] The positive charged Fe irons can repress the three-body collisions and therefore the nucleation process. However, with a weakened magnetic field configuration when the backing plate is used, the suppression by the Fe cations to the cluster nucleation is reduced so that a higher nuclei density can be obtained, which results in smaller NPs at the same free metal flux owing to a lower ratio of free metal density to the density of nuclei in the cluster growth area. The nuclei then grow larger following two models: (i) a successive absorption of free metal atoms and (ii) a cluster-cluster collision growth.[29,36]

At the beginning of cluster growth, an atomic vapor condensation growth ($Fe_q + Fe \rightarrow Fe_{q+1}$) is the dominant process. Particle growth by this kind of single atom addition can also be influenced by the aforementioned charge of the sputtered Fe atoms. As it was reported elsewhere,[21] a high fraction of clusters prepared by plasma sputtering are ionized, and most of them are negatively charged probably due to electron attachment based on Marek's report.[37] In this case, the negatively charged clusters attract the positive Fe ions. Comparing with the high ionization ratio in a high magnetic field where electronic attraction can boost the single atom addition, particle growth following this mode is suppressed with the backing plate present due to the low ionization ratio of the free metal atoms. Furthermore, as the clusters grow up to a certain size and the density is high enough for coalescence, collisions between clusters ($Fe_m + Fe_n \rightarrow Fe_{m+n}$) gradually develop into the decisive process for NP growth. This will, to a large extent, speed up the increase of NP size. As the reduced magnetic field strength results in a weakened magnetic confinement, smaller clusters are able to escape from the area between the anode and cathode, which are subsequently carried by Ar collisions through the aggregation chamber.

As sputtering proceeds, both the aggregation length and the race-track formed on the sputtering target influence the final particle size. The increase of the aggregation length and the depth of the race-track are both supposed to trigger the formation of larger clusters.[25,38] Nevertheless, during the experiments, some uncommon size evolutions are observed. Figure 4 shows the combined influence of the increasing aggregation length and the depth of the race-track on NP size for two groups of experiment with significantly different backing plate thicknesses (0. 5 and 1.5 mm). Both groups of data show more a non-monotonic tendency for the NP size to evolve instead of a gradual increasing trend. This abnormal relationship can possibly be attributed to the varying interference of the magnetic field by the Fe target on the magnetic field configuration from the magnetron head. Indeed, as the experiment continues, the sputtered region goes closer to the magnetron head and a continuously strengthened plasma confinement leads to an increasingly narrowed race-track. In this case, a varied magnetic inference can be expected from the constantly eroded Fe target, which in turn will have impact on the magnetic field distribution and the subsequent sputtering progress. Nevertheless, a substantial increase of the aggregation length will definitely engender a larger particle size, as the linear fitting indicates an overall upward tendency. The morphology evolution of NPs for different sizes is also indicated in Figure 4 by the inserted particle shapes to illustrate in more detail the associated changes.

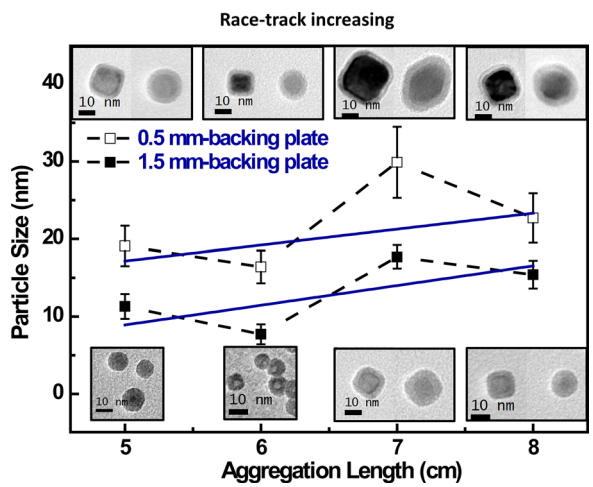

FIG. 4. NP size evolution influenced by an increased aggregation length and an increasing width of the race-track on the iron target (the corresponding NP morphologies are shown as insets based on a large number of area surveys performed). Data are shown for two different backing plate thicknesses (0.5 and 1.5 mm). The lines show the linear fitting of each data set.

IV. CONCLUSIONS

In summary, tunable-sized Fe and Fe-oxide NPs were prepared by manipulating the magnetic field configuration using a non-magnetic metal backing plate in between the sputtering target and the magnetron head in the NP deposition system. The particle shape and structure also experience an evolution varying from faceted morphologies (truncated cube and truncated rhombic dodecahedron) with a core-shell structure for NPs with sizes larger than ~15 nm, to core-shell structured near-spherical polyhedral shapes for NPs with sizes ~8–15 nm, and to homogeneous fully oxidized NPs adopting a near-spherical shape. The modified magnetic field configuration above the target is realized to further facilitate the sputtering process of the magnetic Fe target material. The smaller NPs produced by using the backing plates can be attributed to a lower fraction of ionized free Fe atoms that results in a higher nuclei density, as well as a weakened magnetic confinement that allows NPs with smaller size to escape. Our results provide a simple but effective manner to further control the size, structure, and morphology of Fe NPs and the otherwise difficult-to-sputter magnetic materials.

SUPPLEMENTARY MATERIAL

See supplementary material for the schematic of cluster source.

ACKNOWLEDGMENTS

We are grateful for the support by the Zernike Institute for Advanced Materials. We also gratefully acknowledge the China Scholarship Council for financial support (of L.X.).

[1]B. D. Terris and T. Thomson, J. Phys. D: Appl. Phys. **38**, R199 (2005).
[2]H. M. T. Galvis, J. H. Bitter, C. B. Khare, M. Ruitenbeek, A. I. Dugulan, and K. P. de Jong, Science **335**, 835 (2012).
[3]J.-M. Yan, X.-B. Zhang, S. Han, H. Shioyama, and Q. Xu, Angew. Chem. **120**, 2319 (2008).
[4]A. B. Cundy, L. Hopkinson, and R. L. D. Whitby, Sci. Total Environ. **400**, 42 (2008).
[5]B. Chertok, B. A. Moffat, A. E. David, F. Yu, C. Bergemann, B. D. Ross, and V. C. Yang, Biomaterials **29**, 487 (2008).
[6]B. Chertok, A. E. David, and V. C. Yang, Biomaterials **31**, 6317 (2010).
[7]C. G. Hadjipanayis, M. J. Bonder, S. Balakrishnan, X. Wang, H. Mao, and G. C. Hadjipanayis, Small **4**, 1925 (2008).
[8]A. K. Gupta and M. Gupta, Biomaterials **26**, 3995 (2005).
[9]R. Qiao, C. Yang, and M. Gao, J. Mater. Chem. **19**, 6274 (2009).
[10]L. Zhang and T. J. Webster, Nano Today **4**, 66 (2009).

[11]C. de Montferrand, L. Hu, I. Milosevic, V. Russier, D. Bonnin, L. Motte, A. Brioude, and Y. Lalatonne, Acta Biomater. **9**, 6150 (2013).
[12]V. H. Grassian, J. Phys. Chem. C **112**, 18303 (2008).
[13]Z. L. Wang, J. Phys. Chem. B **104**, 1153 (2000).
[14]D. Farrell, S. A. Majetich, and J. P. Wilcoxon, J. Phys. Chem. B **107**, 11022 (2003).
[15]S. Peng, C. Wang, J. Xie, and S. Sun, J. Am. Chem. Soc. **128**, 10676 (2006).
[16]A. Shavel, B. Rodríguez-González, M. Spasova, M. Farle, and L. M. Liz-Marzán, Adv. Funct. Mater. **17**, 3870 (2007).
[17]C. J. Choi, O. Tolochko, and B. K. Kim, Mater. Lett. **56**, 289 (2002).
[18]Y. Saito, K. Mihama, and R. Uyeda, Jpn. J. Appl. Phys., Part 1 **19**, 1603 (1980).
[19]C. Wang, D. R. Baer, J. E. Amonette, M. H. Engelhard, J. Antony, and Y. Qiang, J. Am. Chem. Soc. **131**, 8824 (2009).
[20]J. Zhao, E. Baibuz, J. Vernieres, P. Grammatikopoulos, V. Jansson, M. Nagel, S. Steinhauer, M. Sowwan, A. Kuronen, K. Nordlund, and F. Djurabekova, ACS Nano **10**, 4684 (2016).
[21]H. Haberland, M. Karrais, M. Mall, and Y. Thurner, J. Vac. Sci. Technol., A **10**, 3266 (1992).
[22]L. Xing, G. H. ten Brink, B. Chen, F. P. Schmidt, G. Haberfehlner, F. Hofer, B. J. Kooi, and G. Palasantzas, Nanotechnology **27**, 215703 (2016).
[23]W. Posadowski, Vacuum **46**, 1017 (1995).
[24]P. J. Kelly and R. D. Arnell, Vacuum **56**, 159 (2000).
[25]M. Hennes, A. Lotnyk, and S. G. Mayr, Beilstein J. Nanotechnol. **5**, 466 (2014).
[26]S. D. Ekpe, F. J. Jimenez, D. J. Field, M. J. Davis, and S. K. Dew, J. Vac. Sci. Technol., A **27**, 1275 (2009).
[27]S. A. Koch, Ph.D. thesis, University of Groningen, 2005.
[28]S. Yamamuro, K. Sumiyama, and K. Suzuki, J. Appl. Phys. **85**, 483 (1999).
[29]T. Hihara and K. Sumiyama, J. Appl. Phys. **84**, 5270 (1998).
[30]Y. Yin, Science **304**, 711 (2004).
[31]A. Cabot, V. F. Puntes, E. Shevchenko, Y. Yin, L. Balcells, M. A. Marcus, S. M. Hughes, and A. P. Alivisatos, J. Am. Chem. Soc. **129**, 10358 (2007).
[32]D. A. J. Herman, P. Ferguson, S. Cheong, I. F. Hermans, B. J. Ruck, K. M. Allan, S. Prabakar, J. L. Spencer, C. D. Lendrum, and R. D. Tilley, Chem. Commun. **47**, 9221 (2011).
[33]L. Signorini, L. Pasquini, L. Savini, R. Carboni, F. Boscherini, E. Bonetti, A. Giglia, M. Pedio, N. Mahne, and S. Nannarone, Phys. Rev. B **68**, 195423 (2003).
[34]A. Pratt, L. Lari, O. Hovorka, A. Shah, C. Woffinden, S. P. Tear, C. Binns, and R. Kröger, Nat. Mater. **13**, 26 (2014).
[35]K. R. Bray, C. Q. Jiao, and J. N. DeCerbo, J. Vac. Sci. Technol., B **32**, 031805 (2014).
[36]J. M. Soler, N. García, O. Echt, K. Sattler, and E. Recknagel, Phys. Rev. Lett. **49**, 1857 (1982).
[37]A. Marek, J. Valter, S. Kadlec, and J. Vyskočil, Surf. Coat. Technol. **205**(Supplement 2), S573 (2011).
[38]M. Ganeva, A. V. Pipa, and R. Hippler, Surf. Coat. Technol. **213**, 41 (2012).